Observation of Excitonic N-Body Bound States: Polyexcitons in Diamond

J. Omachi,[1,2] T. Suzuki,[2,3] K. Kato,[2,3] N. Naka,[4] K. Yoshioka,[2,5] and M. Kuwata-Gonokami[1,2,5,*]

[1]*Photon Science Center, The University of Tokyo, 7-3-1 Hongo, Bunkyo-ku, Tokyo 113-8656, Japan*
[2]*Core Research for Evolutional Science and Technology (CREST), JST, 7-3-1 Hongo, Bunkyo-ku, Tokyo 113-8656, Japan*
[3]*Department of Applied Physics, The University of Tokyo, 7-3-1 Hongo, Bunkyo-ku, Tokyo 113-8656, Japan*
[4]*Department of Physics, Kyoto University, Kitashirakawa, Sakyo-ku, Kyoto 606-8502, Japan*
[5]*Department of Physics, The University of Tokyo, 7-3-1 Hongo, Bunkyo-ku, Tokyo 113-0033, Japan*

(Received 2 May 2013; published 9 July 2013)

We have found a series of resonances associated with the bound state (polyexcitons, PE^Ns) of N excitons up to $N = 6$ in the emission spectra of diamond under two-photon excitation at around 10 K. Time-resolved spectra show a stepwise formation of PE^Ns with smaller to larger N, as well as a successive decay from larger to smaller N. At higher excitation levels, the transformation of PE^Ns into a condensed phase of electron-hole droplets occurs. The binding energies of the PE^Ns, normalized to the exciton Rydberg energy, agree well with those of silicon, suggesting the universality of the phenomena.

DOI: 10.1103/PhysRevLett.111.026402 PACS numbers: 71.35.Lk, 78.47.jd, 78.55.Ap

The ensemble of electrons and holes in a photoexcited semiconductor shows various phases, such as excitons, biexcitons, and electron-hole plasma [1], depending on the density and temperatures. The relatively long recombination lifetimes of electrons and holes in indirect-gap semiconductors provide an opportunity to explore the many-body quantum physics of such an excitonic matter phase. In addition, the band degeneracy in indirect-gap semiconductors stabilizes a dense electron-hole liquid phase [2]. It is well known that excitons spatially condense to form a macroscopic liquid state called electron-hole droplets (EHDs), under high-excitation conditions below the critical temperature T_c.

The droplet formation is governed by thermal collection of excitons on a droplet surface and by the evaporation loss of excitons within the carrier recombination time [3]. Below a certain temperature T_b ($< T_c$) the thermal velocity of the excitons is so low that droplets cannot grow large enough by collecting excitons within the recombination time [4,5]. Under the condition, therefore, the system becomes an intriguing arena of low-temperature, few-body excitonic states.

Quantum mechanics of such few-body systems is, in general, an important research field connecting single-particle quantum mechanics to many-body physics. For example, Efimov reported the appearance of three-body bound states with the universal and peculiar features of resonantly interacting few-body boson systems [6]. Recent experiments with cold atoms have stimulated the study of few-body quantum systems and have extended the interest of this research area to more complex systems in broader fields, including chemistry, nuclear physics, and also solid-state physics [7].

Since excitons are also bosonic quasiparticles, the quest for the existence of N-exciton bound states is an important fundamental problem. They are considerably more complex and nontrivial compared with well-known states, such as biexcitons, electron-hole plasma, and EHDs. In a quasi-one-dimensional charge-transfer crystal, the Coulomb attraction between polarized charge-transfer excitons stabilizes the N-exciton bound states (called exciton N-strings) and such states have actually been observed [8]. In a conventional direct-gap bulk semiconductor, however, bound states containing more than two excitons are unstable because of Pauli blocking effects. On the other hand, Wang and Kittel examined the stability of bound states of N excitons, that is, polyexciton states PE^Ns in an indirect-gap semiconductor with valley degeneracy. The multivalley nature of the conduction electrons relaxes the Pauli blocking effect and stabilizes a PE composed of up to $N = 2m$ excitons with two possible spin orientations, where m is the number of valleys [9]. The signatures of PEs as intrinsic free composite particles have been observed in high-purity silicon crystals [10,11]. However, the small binding energy prevents systematic studies well below $T_b = 9$ K. This limitation caused some controversial discussions on the existence of PEs in semiconductors [12]. Therefore, the nature of PEs has not yet been well explored to date.

In this Letter, we report on the observation of PEs and their formation dynamics in diamond. In this material, a wide-band indirect-gap semiconductor, the critical temperature for EHD formation is as high as 165 K and the density of carriers inside an EHD is about 10^{20} cm^{-3}. Auger-type many-body decay processes shorten the carrier lifetime to the order of 1 ns [13], and such rapid carrier recombination prevents the growth of large droplets. A classical nucleation theory predicts $T_b = 60$ K [14] for diamond which is much higher than for silicon and germanium. This is beneficial for the formation of PEs in diamond because it is essential to prepare electrons and holes well below T_b. We fulfilled this requirement by applying a

two-photon excitation method, instead of one-photon excitation with which the electron temperature is normally raised by 15–30 K [15]. To prepare electrons and holes well below T_b, we set the lattice temperature around 10 K. Consequently, we observed new photoluminescence lines spectrally located below the free-exciton emission. The excitation-density dependence of the luminescence reveals that the new lines are due to the phonon-assisted radiative recombination of an exciton in a PE^N, which leaves a PE^{N-1}. Furthermore, the temporal profiles show features characterizing the formation and decay processes of PE^Ns in the pico- to nanosecond time scales. These results clearly evidence the existence of PE^Ns in diamond, and support the experimental findings of PE^Ns in time-integrated luminescence spectra in silicon.

We used type-IIa, high-purity single crystals of diamond, grown by the high-pressure, high-temperature method. The excitation light source was the third-harmonic of a near-infrared beam from a regenerative amplifier of a Ti:sapphire laser system operated at 1 kHz. The pulse width was about 100 fs. Although the excitation photon energy (4.9 eV) was smaller than the band gap energy of diamond (5.49 eV), electron-hole pairs were produced by two-photon absorption processes. The maximum achievable density is 4.8×10^{18} cm^{-3}, which is below a damage threshold [16]. In this Letter, we limit our discussion to densities below 2.5×10^{16} cm^{-3}, which is $1/(4 \times 10^3)$ of the density of electron-hole pairs inside an EHD. In this rather moderate two-photon excitation regime, we can keep the homogeneity of the carrier distribution along the sample depth and avoid the collision-induced heating of carriers [15]. The luminescence from the sample was collected in backscattering geometry, and detected either by a cooled CCD camera placed behind a 50 cm spectrometer (Acton Research Co., SP500) or by a streak camera system (Hamamatsu, M5676 and C5094) with temporal resolutions of 0.12 or 1.5 ns, in accordance with the time scales set.

Figure 1(a) shows time-integrated photoluminescence spectra at various excitation intensities. The strongest peak, observed around 5.27 eV, is due to the transverse-optical (TO)-phonon-assisted recombination of free excitons [13]. We extracted the excitonic temperature (T_{ex}) by fitting the line shape assuming a Maxwell-Boltzmann distribution, including the spectral resolution of the detection system [13]. We obtained $T_{ex} \leq 14$ K, except for the highest excitation density ($= 69n'$, where $n' = 3.1 \times 10^{14}$ cm^{-3}), where the tail of the exciton emission was slightly broadened by the collision-induced heating of carriers.

The bottom spectrum at the lowest excitation density $n = 9 \times 10^{12}$ cm^{-3} ($= n'/33$) clearly shows longitudinal-optical (LO)-phonon-assisted recombination of free excitons at 5.24 eV [13]. There is also a small peak at 5.21 eV, which results from the TO-phonon-assisted recombination of excitons bound to boron sites [17]. Upon increasing the

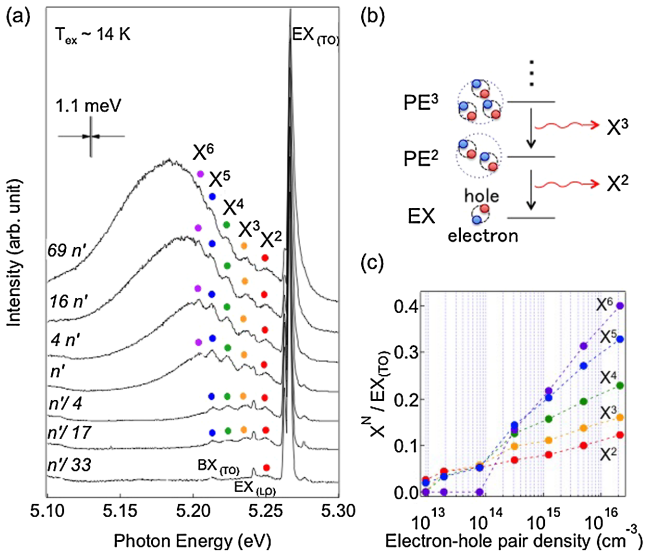

FIG. 1 (color online). (a) Time-integrated photoluminescence spectra at $T_{ex} \sim 14$ K at various excitation intensities. The average density of the electron-hole pairs is indicated in units of $n' = 3.1 \times 10^{14}$ cm^{-3}. (b) Schematic diagram of the radiative decay of an exciton following the transition from the PE^N state to the PE^{N-1} state. (c) Excitation-density dependence of the peak intensity of the X^N ($N = 2$–6) line normalized to that of the $EX_{(TO)}$ emission.

excitation intensity, discrete emission peaks start to appear at the low-energy side of the TO-phonon-assisted emission of free excitons. The number of peaks increases with the density, and we observed up to five discrete peaks, as marked by the solid circles in Fig. 1(a). The overall line shape is similar to that of the PE emission in silicon [11]. We labeled each peak component as the X^2, X^3, X^4, X^5, and X^6 lines, from higher to lower energy, following the notations for PE emission in silicon [10]. We attribute each peak of the emission to a transition from the PE^N state to the PE^{N-1} state with emission of a photon and a TO phonon, as shown in Fig. 1(b). It should be noted that the observed X^2–X^4 lines appear at higher energies than the emission of bound excitons at 5.21 eV. This implies that the observed X^N lines originate from emission associated with intrinsic freely propagating multiexcitons, rather than from the recombination of a bound multiexciton complex [18].

The spectra in Fig. 1(a) show three remarkable features. One is that the peak positions of X^N are almost independent of the excitation density or the average density of electron-hole pairs. This feature is significantly different from what is observed for the EHD emission, where the spectral positions of the EHD emission depend on the carrier density and the droplet size [2]. We have listed the peak energies of the X^N lines in the first row of Table I. To estimate the binding energies of the N-exciton bound states, we calculated the energy separations between the peak position of the X^N line and the low-energy edge [$E_{EX_{(TO)}} = 5.262$ eV] of the

TABLE I. Spectral and temporal properties of the X^N lines. First row: peak energies of the X^N lines. Second row: energy interval between the X^N peak and the low-energy edge [$E_{\mathrm{EX}_{(\mathrm{TO})}} = 5.262$ eV] of the free-exciton emission, normalized by the exciton binding energy (0.08 eV). Third row: binding energy of PE^N, normalized by the binding energy of the exciton (14.7 meV) in silicon [11]. Fourth row: rise time τ_R of the X^N line. Fifth row: peak time τ_P or the time at which the X^N emission reaches its maximum level. For the X^5 line, spectral overlaps with the bound-exciton emission caused errors in the determination of the rise and peak times.

	X^2	X^3	X^4	X^5	X^6
Energy (eV)	5.250	5.237	5.225	5.214	5.204
$(\mathrm{EX} - X^N)/R$ in diamond	0.15	0.31	0.46	0.60	0.73
$(\mathrm{EX} - X^N)/R$ in silicon [11]	0.10	0.30	0.46	0.55	0.66
τ_R (ns)	0.42	0.44	0.50	(0.52)	0.52
τ_P (ns)	0.55	0.77	0.81	(1.00)	0.95

free-exciton emission. The values, normalized by the exciton binding energy ($R = 80$ meV), are shown in the second row of Table I. We also compared these normalized binding energies in diamond with those in silicon [11], which are shown in the third row of Table I. As we can see from the table, the series of binding energies show excellent agreements. These findings suggest that the two systems share a common, universal underlying physics on the N-body bound states of excitons.

The second feature in Fig. 1(a) is that the entire emission line has a low-energy tail, which can be explained by the sum of the low-energy tails of the individual X^N lines representing the emission from PE^Ns with finite kinetic energy, as is usually observed for the biexciton emission [19,20]. When the average density of the electron-hole pairs is above 5×10^{15} cm^{-3} ($= 16n'$), the low-energy tail merges into an EHD-like broadband spectrum, as shown in the two upper spectra in Fig. 1(a). The spectral position of the EHD-like band is slightly shifted to higher energies compared to the typical EHD emission band [13,21], which indicates a small droplet size [2].

The third feature is that the X^N line intensity increases nonlinearly with the density, as shown in Fig. 1(c). We note spectral overlaps due to the low-energy tails of the higher-energy lines and of the X^5 line with the bound-exciton emission. Nevertheless, it is clear that lower-energy components grow faster than higher-energy ones upon increasing the density. This can be interpreted as a lower-energy emission line originating from a PE^N state with larger N. In summary, the three spectral features described above indicate that the group of emission lines is due to the recombination of PE^Ns.

Figure 2 shows a streak-camera image of the time-resolved photoluminescence signal at $T_{\mathrm{ex}} = 13$ K and $n = 1.6 \times 10^{15}$ cm^{-3} ($= 5.2n'$). The ordinate shows the time delay after photoexcitation, and the abscissa is the photon energy. The trace at the bottom is the time-integrated photoluminescence spectrum. The image shows stripes along the time delay at each X^N line. The temporal profiles and the spectral positions of the PE bands are significantly different from those of the EHD emission [13,22].

The curves in Fig. 3(a) are temporal profiles of the exciton and X^N line intensities measured at a temporal resolution of 0.12 ns, within an energy range of ±4 meV around each peak. The intensity has been normalized to the maximum value, and we define the time origin as the time at which exciton emission emerges. The dashed red curve in Fig. 3(a) shows the temporal profile of the overall PE emission for the energy range from 5.144 to 5.262 eV. It can be seen that the exciton emission first appears, and then reaches a maximum value at 0.39 ns. The overall intensity of the PE emission reaches a peak value directly after a

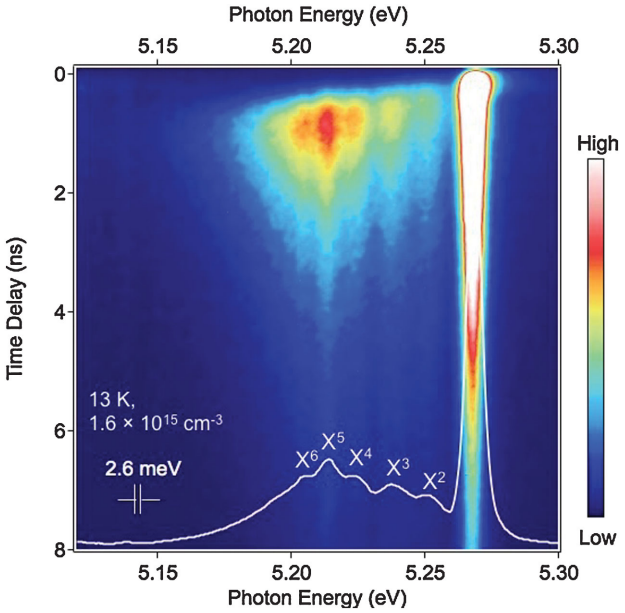

FIG. 2 (color). Time-resolved photoluminescence image at $T_{\mathrm{ex}} = 13$ K and $n = 1.6 \times 10^{15}$ cm^{-3} ($= 5.2n'$), measured using a streak camera system. The ordinate shows the time delay after photoexcitation, and the abscissa is the photon energy. The temporal resolution is 0.12 ns. The trace at the bottom is the photoluminescence spectrum integrated over time.

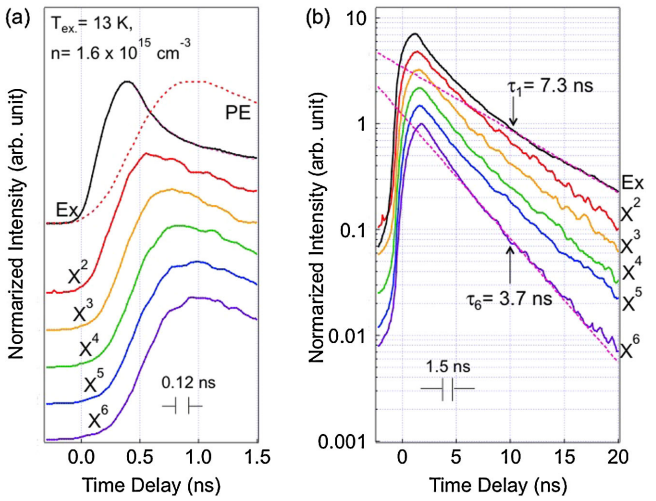

FIG. 3 (color online). Temporal profiles of the emission intensities of the exciton (Ex) and the PE^N (a) within the first 1.5 ns and (b) up to 20 ns at $T_{ex} = 13$ K and $n = 1.6 \times 10^{15}$ cm^{-3} ($= 5.2n'$).

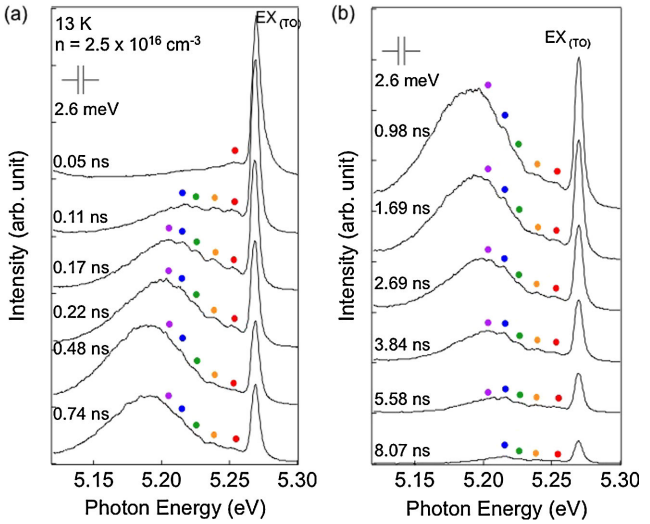

FIG. 4 (color online). Temporal evolution of the PE emission and EHD-like broadband emission spectra at $T_{ex} = 13$ K and $n = 2.5 \times 10^{16}$ cm^{-3}($= 81n'$) showing (a) the formation and (b) the decay dynamics. The delay times are shown on the left-hand side of each panel. The spectra have been averaged over the temporal resolution of the measurements, which is 0.06 ns and 0.12 ns for (a) and (b), respectively. The solid circles indicate discrete emission peaks of PE^Ns.

steep fall of the exciton emission. On the other hand, the PE emission appears after a finite delay time. The rise and peak times for each X^N line are summarized in the fourth and fifth rows of Table I, where the rise time is defined as the time difference between 10% and 90% of the maximum level. A step-by-step appearance from the X^2 to the X^6 line is now clear. For the X^5 line, a spectral overlap with the bound-exciton emission caused errors in the determination of the rise and peak times. Figure 3(b) shows the decay dynamics of the PE emission measured at a temporal resolution of 1.5 ns. Since the decay curves are not single exponential, we extract the characteristic decay times from the slope at 10 ns for the exciton ($\tau_1 = 7.3$ ns) and for the X^6 line ($\tau_6 = 3.7$ ns). It can be seen that the emission of PE^Ns with larger N decays faster, but detailed processes of the N-dependent decay are still unclear. We believe that these experimental results can give insights into the few-body physics of the electron-hole systems and the connections between few-body and many-body systems.

Furthermore, we investigated the relation between PEs and EHDs at low temperatures. Figure 4 shows the temporal evolution of the emission spectra at $T_{ex} = 13$ K and $n = 2.5 \times 10^{16}$ cm^{-3} ($= 81n'$). The spectra are averaged over 0.06 and 0.12 ns in Figs. 4(a) and 4(b), respectively. We can see that at first the PE emission rises (depicted by the solid circles in Fig. 4), and then the low-energy tail of the PE emission merges into a broadband spectrum after 0.48 ns. The broadband emission, ranging from 5.120 to 5.195 eV, is characterized by a single-exponential decay with a decay constant of 1.5 ns, which is slightly longer than that of the EHD emission (~ 1 ns [13]) but shorter than those of the X^N lines. These features in the temporal evolution of the spectra suggest that the PE^Ns of a larger but finite N transform into a condensed phase of EHDs. Theoretically, Wang and Kittel pointed out that N is limited to the number of the band degeneracy ($N = 12$ including spins in diamond), according to the Pauli blocking effects [9]. Here we cannot resolve PE^Ns with $N > 6$, possibly because of spectral overlap. The formation of EHDs from PEs is an interesting fusion process in an electron-hole system at low temperatures, where quantum mechanics could play an important role.

Finally we discuss the theoretical aspects of the stability of PEs. Although the concept of PEs is well accepted, their stability is theoretically unresolved because of the difficulty of calculating their binding energies [23,24]. Morgan pointed out qualitatively that stable PE^Ns up to at least $N = 6$ can be formed in silicon, based on the hydrogenlike model, taking into account the antisymmetric combination of wave functions of valleys and the anisotropy of conduction bands [25]. Both for silicon [11] and diamond (this work), which have similar band structures, the experiments have shown signatures of PE^Ns up to $N = 6$.

In conclusion, we observed emission associated with N-exciton bound states PE^Ns up to $N = 6$ in diamond under two-photon interband excitation preparing the cold excitons around 14 K. The temporal profiles of the PE^N signals show characteristic features, stepwise formation, and a faster decay of the PE^Ns with larger N. The excellent agreement between the normalized binding energies of PE^Ns in silicon and diamond suggests the universality of the underlying physics regarding the appearance of N-exciton bound states, as discussed by Efimov for resonantly interacting boson systems. Further experimental studies on PE^N states and a detailed comparison with

theory are in progress. At a higher excitation level, time-resolved data suggest that PEs transform into EHDs. A systematic study within a wider range of excitation densities and temperatures is crucial to connect the few-body phenomena to many-body physics. This will provide an opportunity to reveal an overall phase diagram of excitonic matter in semiconductors.

We are grateful to S. Endo and M. Horikoshi for helpful discussions. We thank H. Sumiya (Sumitomo Electric Industries, Ltd.) for providing the samples. This work was supported by Grant-in-Aid for Scientific Research on Innovative Area "Optical Science of Dynamically Correlated Electrons (DYCE)," No. 20104002, Project for Developing Innovation Systems, and Photon Frontier Network Program of the Ministry of Education, Culture, Sports, Science, and Technology, Japan, and Funding Program for World-Leading Innovative R&D on Science and Technology (FIRST) of Japanese Society for the Promotion of Science, Japan.

*gonokami@phys.s.u-tokyo.ac.jp

[1] C. Klingshirn, *Semiconductor Optics* (Springer-Verlag, Berlin, 2005), 2nd ed.
[2] *Electron-Hole Droplets in Semiconductors*, edited by C. D. Jeffries and L. V. Keldysh (North-Holland, Amsterdam, 1983).
[3] R. M. Westervelt, Phys. Status Solidi B **74**, 727 (1976).
[4] R. N. Silver, Phys. Rev. B **11**, 1569 (1975).
[5] M. Combescot and R. Combescot, Phys. Lett. **56A**, 228 (1976).
[6] V. N. Efimov, Yad. Fiz. **12**, 1080 (1970) [Sov. J. Nucl. Phys. **12**, 589 (1971)].
[7] For a review, see F. Ferlaino and R. Grimm, Physics **3**, 9 (2010).
[8] M. Kuwata-Gonokami, N. Peyghambarian, K. Meissner, B. Fluegel, Y. Sato, K. Ema, R. Shimano, S. Mazumdar, F. Guo, T. Tokihiro, H. Ezaki, and E. Hanamura, Nature (London) **367**, 47 (1994).
[9] J. S. Wang and C. Kittel, Phys. Lett. **42A**, 189 (1972).
[10] A. G. Steele, W. G. McMullan, and M. L. W. Thewalt, Phys. Rev. Lett. **59**, 2899 (1987).
[11] M. L. W. Thewalt, in *Proceedings of the 23rd ICPS*, edited by M. Scheffler and R. Zimmermann (World Scientific, Singapore, 1996), Vol. 1, p. 381.
[12] There was a claim that the results originate from a condensed phase of electron-hole plasma [L. M. Smith and J. P. Wolfe, Phys. Rev. B **51**, 7521 (1995)].
[13] R. Shimano, M. Nagai, K. Horiuch, and M. Kuwata-Gonokami, Phys. Rev. Lett. **88**, 057404 (2002).
[14] J. H. Jiang, M. W. Wu, M. Nagai, and M. Kuwata-Gonokami, Phys. Rev. B **71**, 035215 (2005).
[15] N. Naka, T. Kitamura, J. Omachi, and M. Kuwata-Gonokami, Phys. Status Solidi B **245**, 2676 (2008).
[16] S. Preuss and M. Stuke, Appl. Phys. Lett. **67**, 338 (1995).
[17] N. Naka, J. Omachi, H. Sumiya, K. Tamasaku, T. Ishikawa, and M. Kuwata-Gonokami, Phys. Rev. B **80**, 035201 (2009).
[18] Ya. E. Pokrovskii, Phys. Status Solidi A **11**, 385 (1972).
[19] K. Cho, Opt. Commun. **8**, 412 (1973).
[20] I. Pelant and J. Valenta, *Luminescence Spectroscopy of Semiconductors* (Oxford University, New York, 2012).
[21] K. Thonke, R. Schliesing, N. Teofilov, H. Zacharias, R. Sauer, A. M. Zaitsev, H. Kanda, and T. R. Anthony, Diam. Relat. Mater. **9**, 428 (2000).
[22] M. Nagai, R. Shimano, K. Horiuchi, and M. Kuwata-Gonokami, Phys. Rev. B **68**, 081202(R) (2003).
[23] W. F. Brinkman, T. M. Rice, and B. Bell, Phys. Rev. B **8**, 1570 (1973).
[24] A. C. Cancio and Yia-Chung Chang, Phys. Rev. B **42**, 11317 (1990).
[25] T. N. Morgan, Nuovo Cimento Soc. Ital. Fis. **39B**, 602 (1977).